European Journal of Pharmaceutical Sciences 185 (2023) 106440

Contents lists available at ScienceDirect

European Journal of Pharmaceutical Sciences

journal homepage: www.elsevier.com/locate/ejps

Effect of different seed crystals on the supersaturation state of ritonavir tablets prepared by hot-melt extrusion

Hengqian Wu [a,b], Zhengping Wang [b,c], Yanna Zhao [b], Yan Gao [a], Lili Wang [a], Heng Zhang [a], Rupeng Bu [b], Zhuang Ding [b], Jun Han [b,a,c,*]

[a] School of Chemistry and Chemical Engineering, University of Jinan, Jinan, Shandong, 250022, China
[b] Institute of BioPharmaceutical Research, Liaocheng University, Liaocheng, Shandong, 252059, China
[c] Liaocheng High-Tech Biotechnology Co., Ltd., Liaocheng, Shandong, 252059, China

ARTICLE INFO

Keywords:
Amorphous solid dispersion
Hot-melt extrusion
Ritonavir
Seed crystals
Crystal growth
Supersaturated solution

ABSTRACT

Hot-melt extrusion (HME) is a technology increasingly common for the commercial production of pharmaceutical amorphous solid dispersions (ASDs), especially for poorly water-soluble active pharmaceutical ingredients (APIs). However, recrystallization of the APIs during dissolution must be prevented to maintain the supersaturation state enabled by ASD. Unfortunately, the amorphous formulation may be contaminated by seed crystals during the HME manufacturing process, which could lead to undesirable crystal growth during the dissolution process. In this study, the dissolution behavior of ritonavir ASD tablets prepared using both Form I and Form II polymorphs was examined, and the effects of different seed crystals on crystal growth rates were investigated. The aim was to understand how the presence of seed crystals can impact the dissolution of ritonavir, and to determine the optimal polymorph and seeding conditions for the production of ASDs. The results showed that both Form I and Form II ritonavir tablets had similar dissolution profiles, which were also similar to the reference listed drug (RLD). However, it was observed that the presence of seed crystals, particularly the metastable Form I seed, led to more precipitation compared to the stable Form II seed in all formulations. The Form I crystals that precipitated from the supersaturated solution were easily dispersed in the solution and could serve as seeds to facilitate crystal growth. On the other hand, Form II crystals tended to grow more slowly and presented as aggregates. The addition of both Form I and Form II seeds could affect their precipitation behaviors, and the amount and form of the seeds had significant effects on the precipitation process of the RLD tablets, as are the tablets prepared with different polymorphs. In conclusion, the study highlights the importance of minimizing the contamination risk of seed crystals during the manufacturing process and selecting the appropriate polymorph for the production of ASDs.

1. Introduction

For oral dosage forms, the improved solubility of poorly water-soluble drugs is critical to reaching desirable systemic exposure (Amidon et al., 1995). Several strategies have been developed to improve the solubility and bioavailability of those drugs, such as co-crystals, complexation, salt formation, nanonization, liposomes, pH micro-environmental modifiers, soft gel capsules, amorphous solid dispersion (ASD), etc. (Choi et al., 2017; Fenske et al., 2008; Mohammadian et al., 2019; Proietti et al., 2014; Reggane et al., 2018; Serajuddin, 2007; Stephenson et al., 2011; Wong et al., 2018). Salt formation to improve solubility only works with 20–30% of weakly acidic and basic drugs (Jermain et al., 2018; Thakral et al., 2016; Zannou et al., 2007). Other methods, such as co-crystals and complexation, may increase crystalline solubility at the expense of decreasing apparent permeability, negating the solubility advantages (Miller et al., 2012). Although there are studies highlighting that ASDs may not always be advisable for improving permeation when solubilization occurs (Raina et al., 2015), ASD is still an attractive option for enhancing both solubility and absorption due to its high thermodynamic activity in supersaturated states (Dahan et al., 2013). Therefore, ASD is widely used to improve drug dissolution and absorption for poorly water-soluble compounds. Over 20 drugs using ASD technology have been approved, according to data from the FDA database (Tambe et al.,

* Corresponding author.
E-mail address: junhanmail@163.com (J. Han).

https://doi.org/10.1016/j.ejps.2023.106440
Received 13 January 2023; Received in revised form 10 March 2023; Accepted 30 March 2023
Available online 31 March 2023

2022). ASD is commonly formulated into a single-phase amorphous mixture that inhibits the recrystallization of the amorphous drug by dispersing it within an amphiphilic polymeric matrix. The molecular dispersion of the drug in a polymer matrix enables a negligible amount of energy to be consumed on lattice disruption during dissolution, as the system finds itself already in a high energy state (Brouwers et al., 2009). Several methods have been documented for the preparation of ASDs, such as spray drying, melting, solvent evaporation, melting solvent, supercritical fluid, and hot-melt extrusion (HME), etc. (Singh and Van den Mooter, 2016; Abuzar et al., 2018; Alzahrani et al., 2022; Goldberg et al., 1966; Sekiguchi and Obi, 1961; Tachibana and Nakamura, 1965). In comparison with other technologies, HME has multiple inherent advantages, including the elimination of organic solvents, homogeneity of mixture, and reduction of processing steps. Therefore, HME is becoming an increasingly commonly used method to produce ASD with twin-screw extruders.

Although considerable progress has been made in ASD technology research, limited numbers of commercial products are found in the US market currently (Li and Taylor, 2018; Solanki et al., 2019). As of 2021, only 27 approved drug products in the US were based on ASD technology (Walden et al., 2021). This may be primarily due to the supersaturation stability of the targeted drugs during dissolution. When ASD dissolves, a “spring effect” can occur, generating a fast supersaturation related to the equilibrium solubility (Guzmán et al., 2007). Drugs dispersed in the bulk aqueous phase surpassing their amorphous solubility separate into in situ amorphous drug-rich nanoparticles. This phenomenon is also referred to as liquid-liquid phase separation (LLPS) (Ilevbare and Taylor, 2013). The LLPS may serve as a reservoir in the supersaturated state to replenish the depleted drug concentration due to permeation (Xu et al., 2017). Meanwhile, LLPS is one of the precursors for drug crystallization. Since both the solubility and absorption flux of the drug are affected by the recrystallization during ASD dissolution, it is necessary to inhibit the recrystallization of the supersaturated solution to achieve a "parachute" state (Guzmán et al., 2007). Therefore, research on the mechanisms of crystal growth is necessary to maintain the supersaturation and bioavailability of the drug (Alonzo et al., 2012).

Ritonavir (Fig. 1A), a poor equilibrium solubility and low membrane permeability drug, is a proteinase inhibitor used for the treatment of human immunodeficiency virus (HIV). It was also used in combination with nirmatrelvir to treat coronavirus disease 2019 (COVID-19) (Lamb, 2022; Sherman and Steinberg, 2011). It is also a polymorphic drug with metastable Form I (Fig. 1B), stable Form II (Fig. 1C), and a newly found least stable Form III via melt crystallization (Yao et al., 2022). The main physicochemical properties of ritonavir were shown in Table 1. Norvir® is a commercially available product that contains ritonavir as API in the form of ASD tablets. Although few publications describe the successful development of Norvir® itself, some research has been directed toward investigating the drug release from ritonavir ASD tablet formulation. Xu et al. assessed in vitro dissolution and supersaturation behaviors of Norvir® oral tablet by two biorelevant dissolution methods with pH alteration, and revealed a high degree of supersaturation of ritonavir from tablets by the occurrence of LLPS in biorelevant dissolution media (Xu et al., 2017). Guo et al. reported that ritonavir tablets disintegrated surprisingly poorly in acidic media when sodium lauryl sulfate (SLS) was used to improve wetting (Guo et al., 2019). Best et al. studied the pharmacokinetics of intact and crushed lopinavir/ritonavir tablets (Kaletra®; Abbvie), which were also manufactured through HME technology, and revealed decreases in the area under the curve (AUC) of 45% and 47% for lopinavir and ritonavir, respectively, if administrating the crushed tablets (Best et al., 2011).

We believe that the amorphous formulation might be contaminated by seed crystals during the manufacturing process (Moseson et al., 2020, 2021). However, few studies have systematically examined the effect of different seed crystals on the recrystallization of supersaturated solutions of ritonavir ASD tablets prepared by HME. Understanding the

Table 1
Main Physicochemical Properties of Ritonavir.

Property	Value/Description	References
pKa	2.01 and 2.51	Guo et al., 2019
logP	5.6	Yu et al., 2020
BCS[a]	IV	Sherman and Steinberg, 2011
Solubility	pH-dependent solubility	Xu et al., 2017
Crystalline form	Form I, Form II, Form III, and Amorphous	Yao et al., 2022

[a] Biopharmaceutical Classification System.

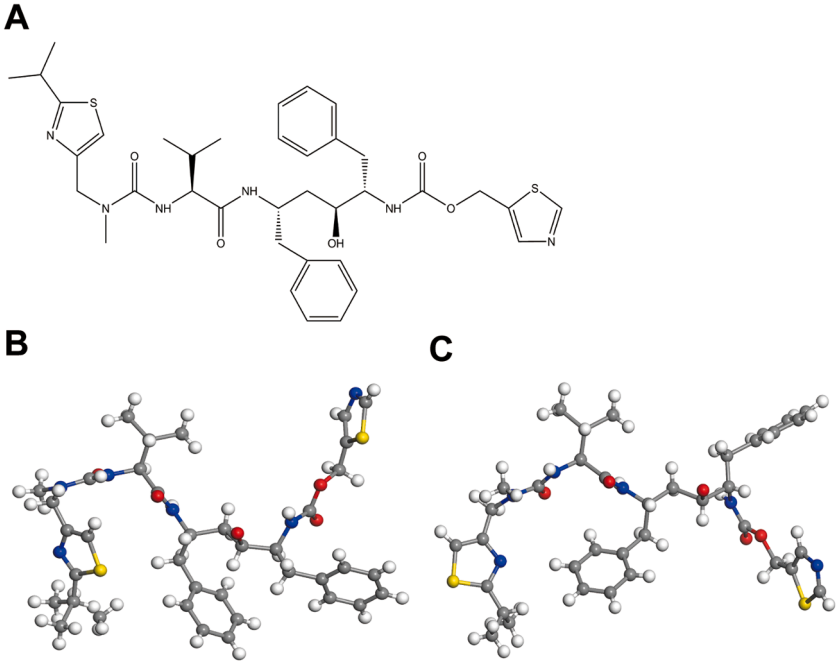

Fig. 1. Molecular structure of ritonavir (A); Molecular conformation of Form I (B) and Form II (C).

impact of different seed crystals on the crystallization rate of the supersaturated solution generated by ritonavir ASD is vital. In this study, two designs were used to systematically investigate the impact of different seed crystals on the recrystallization of the supersaturated solution generated by ritonavir ASD tablets.

The first investigation involved preparing ritonavir tablets with two different polymorphic forms (Form I and Form II) and comparing them with Norvir® ritonavir tablets. This study demonstrated the in vitro equivalence of ritonavir tablets and RLD by dissolution profiles under the sink and non-sink dissolution testing. The second investigation was to study the effect of different seed crystals on the precipitation process of supersaturated solution during the dissolution test by determining particle size, zeta potential, powder X-ray diffraction (PXRD), and polarized light microscope (PLM) observation.

2. Materials and methods

2.1. Materials

Norvir® ritonavir tablet (RLD) was supplied from AbbVie Inc. (North Chicago, USA). Ritonavir ($C_{37}H_{48}N_6O_5S_2$) Form I was purchased from Hetero Drugs Limited (Andhra Pradesh, India), and Form II was obtained from Anhui Biochem United Pharmaceutical Co., Ltd. (Anhui, China) that was used without further purification. Ritonavir Reference Standard (99.3%) was purchased from The United States Pharmacopeial Convention (MD, USA). The ultrapure water was purified by the Milli-Q® Advantage A10® water purification system (Millipore, MA, USA). Acetonitrile of HPLC grade was provided by Thermo Fisher Scientific (Newington, USA). Methanol was purchased from Adamas Pharmaceuticals, Inc. (Shanghai, China). Potassium dihydrogen phosphate and phosphoric acid were obtained from Tianjin Zhiyuan Chemical Reagent Co., Ltd. (Tianjin, China). Polyoxyethylene 10 lauryl ether was obtained by Shanghai Yiji Industrial Co., Ltd. (Shanghai, China). Film Coating Premix (Opadry®, Stomach Dissolving Type) was purchased from Colorcon Inc. (PA, USA). All other experimental excipients were presented in Table 2.

2.2. Determination of equilibrium solubility of Form I and II

To determine the effect of different crystal forms on the solubility of ritonavir, the Form I and II equilibrium solubility were measured using the miniaturized shake-flask solubility method (Guan et al., 2021). Ritonavir powder (Form I or II) in excess amounts was dispersed in a 20 ml volumetric flask containing 5 mL of the following aqueous media in each volumetric flask: HCl solutions at pH 1.2, 2.0, and 3.0; 100 mM acetate buffer at pH 4.0, 4.5, and 5.0; 50 mM phosphate buffer at pH 6.0, 6.8, and 8.0; and water. For equilibrating drug solubility, vials were spun at 100 rpm in an incubator shaker (HNY-2102C, Tianjin Honour Instrument Co., Ltd. Tianjin, China) for 24 h at 37 °C. The pH of suspensions was measured using a pH meter (Five Easy Plus, Mettler Toledo, Zurich, Switzerland) after equilibration. Afterward, the suspensions were filtered through a 0.45 μm poly tetra fluoroethylene (PTFE) syringe filters and saturate the filter with at least 2 mL before collecting a sample. Following appropriate dilutions with corresponding aqueous media, HPLC was used to determine the concentrations of the drugs in different solutions. The solubility studies were conducted in triplicate.

Table 2
The list of ready-to-use excipients.

Excipient Name	Type	Source
PVPVA	Kollidon® VA 64	BASF Corporation, New Jersey, Germany
Sorbitan monolaurate	Span 20-LQ-(AP)	Croda Inc., East Yorkshire, UK
Colloidal Silicon Dioxide	AEROSIL® 200 Pharma	Evonik Degussa GmbH, Essen, Germany
Dibasic Calcium Phosphate Anhydrous	Fujicalin® SG	Fuji Chemical Industries Co., Ltd., Toyama, Japan
Sodium Stearyl Fumarate	Alubra® PG 100	DuPont de Nemours, Inc., Delaware, USA

2.3. Preparation of ritonavir tablets

The quantitative composition of ritonavir 100 mg tablets was following inactive ingredients: 493 mg polyvinylpyrrolidone/vinyl acetate (PVPVA), 90 mg dibasic calcium phosphate anhydrous, 67 mg sorbitan monolaurate, 14 mg colloidal silicon dioxide, 2 mg sodium stearyl fumarate, and 22 mg film coating. Formulation 1 (F1) was prepared from Form I as API, while Formulation 2 (F2) was prepared from Form II. Ritonavir was blended with PVPVA, sorbitan monolaurate, and colloidal silicon dioxide in the manufacturing formula. The blend was extruded in Process 16 Twin-Screw Extruder (Eurolab Pharma 16, Thermo Scientific, MA, USA), and a vacuum was applied to the extruder barrel to degas the melt. The feeding rate of blend in the extruder was 5–10 kg/h, and the screws were rotated at 50–100 rpm at 120 ± 10 °C. The extrudates were calendered by passing through two counter-rotating calender rollers, cooled before milling, and passed through sieve #30 (600 μm opening). The milled extrudates were lubricated with calcium phosphate anhydrous, colloidal silicon dioxide, and sodium stearyl fumarate and compressed into tablets using Performa P rotary press (GEA, Dusseldorf, Germany) to achieve a sufficient hardness (minimum 15 kgf). The length of the punch in the tablet press was 17 mm and the width was 9 mm. The tablets were film coated using BGB-5F Coater (Zhejiang Xiaolun Intelligent Manufacturing Co., Ltd., Zhejiang, China) with film coating premix. The film coating premix were weighed and dissolved in water to achieve a homogenous 10–12% (w/w) solids solution, and finally the solution was filtered to remove any particles. The tablets were placed in the rotating drum and the tablet bed rotated at 5–10 rpm. The coating temperature was between 40 and 50 °C. The coating solution was then atomized into fine droplets using air pressure and sprayed onto the rotating tablet bed. The coating should be at least 3% of the weight of the tablet. After completion of coating solution, the tablets were dried for 20 min at 40–50 °C."

2.4. Sink dissolution testing

The sink dissolution testing of RLD, F1, and F2 was performed using USP dissolution apparatus II (Model Symphony 7100, Distek Inc, North Brunswick, USA) in 900 mL of medium with a stirring speed of 75 rpm at 37 ± 1 °C. The dissolution media used were: 0.1 M hydrochloric acid (pH 1.2), the acetate buffer with 0.06 M polyoxyethylene 10 lauryl ether (pH 4.5), the phosphate buffer with 0.06 M polyoxyethylene 10 lauryl ether (pH 6.8), and water with 0.06 M polyoxyethylene 10 lauryl ether which was based on USP monographs (Law et al., 2004; Sun et al., 2016). Aliquots (5 mL) were withdrawn at predetermined time points of 10, 15, 20, 30, 45, 60, 90, and 120 min to a sampling tube. All collected aliquots from the dissolution apparatus were filtered through a PTFE (0.45 μm) syringe filter to HPLC vials for analysis by HPLC with UV detection. At least 2 mL should be allowed to saturate the filter before collecting the sample. All the dissolution testing was done in triplicates.

2.5. Non-sink dissolution testing with seed crystals

RLD, F1, and F2 were tested for non-sink dissolution using USP dissolution apparatus II in 900 mL of water pre-degassed treatment as the medium with a stirred speed of 75 rpm at 37 ± 1 °C. Aliquots (3 mL) were withdrawn though a 45 micron filter discs (Quality Lab Accessories, PA, USA) at predetermined time points of 10, 15, 20, 30, 45, 60, 90, 120, 150, 180, 210, 240, 270, and 300 min to a sampling tube that contained 2 mL of methanol. The methanol was used to ensure that any supersaturated solution was solubilized prior to analysis. The seed crystals of Form I and Form II were added to the different vessels after 1.0 h of dissolution. Since Form I and Form II seed crystals are

superhydrophobic and their surfaces are not easily wetted (Fig. S1), the solution was immediately stirred with a glass rod after adding the seed crystals to the vessel to disperse them and prevent them from floating on the surface of the dissolution medium as dry powder. The amount of seed crystals added to each dissolution vessels was shown in Table 3. All collected aliquots from the dissolution apparatus were immediately mixed by a mediation oscillator (Vortex-5, Haimen Kylin-Bell Lab Instruments Co., Ltd., Haimen, China) and filtered through a 0.45 μm PTFE syringe filter to HPLC vials for analysis by HPLC with UV detection. At least 2 mL should be allowed to saturate the filter before collecting the sample. After the dissolution test, the precipitates of remaining slurries were collected by suction filtration through a 0.45 μm polyether sulfone (PES) filter. All the dissolution testing was done in triplicates.

2.6. Dissolution profile comparison

The dissolution profiles of F1 and F2 are compared with RLD using a model-independent similarity factor f_2. The similarity factor f_2 is a logarithmic reciprocal square root transformation of the sum of squared errors and measures the similarity between the two dissolution profiles.

$$f_2 = 50 \cdot \log\left\{100 \cdot \left[1 + \frac{1}{n}\sum_{t=1}^{n}(R_t - T_t)^2\right]^{-0.5}\right\}$$

where n is a number of time points, R_t is the dissolution value of the RLD at time t, and T_t is the dissolution value of the test (F1 and F2) at the t time point, $1 \leq t \leq n$. The logarithm in the equation is decadic with base 10. Only one time point was considered after 85% dissolution of tablets in these five dissolution media.

2.7. Ritonavir analysis

Ritonavir concentrations were measured using a Thermo HPLC system (Vanquish, Thermo Scientific, MA, USA). The mobile phase was a mixture of acetonitrile and 30 mM potassium dihydrogen phosphate (55:45 *v/v*, pH 4.0 ± 0.1). It was degassed and filtered through a membrane filter (47 mm × 0.45 μm) prior to use. The samples were injected with a volume of 25 μL at a flow rate of mobile phase 1.5 mL/min. Chromatographic separation was performed at 25 °C using Inertsil C18 column (4.6 × 250 mm). The data was collected and analyzed by HPLC at wavelength 215 nm. A linear calibration curve was obtained in the 10 – 140 μg/mL concentration range with a regression coefficient of 0.999. The standard working solution of ritonavir was prepared using a mixture of methanol and water (50:50 *v/v*) as a dilution medium to 111 μg/mL.

2.8. Particle size measurement

To analyze the particle size of any phase-separated or dispersed drug in the non-filtration sample obtained from the dissolution testing, a Dynamic Light Scattering (DLS) method was employed using the Malvern Nano ZSP instrument (Malvern Instruments, Malvern, UK) at a measurement angle of 173° The instrument was equipped with a He-Ne laser that was set to 37 °C. Before the analysis, the instrument was calibrated with Nanosphere™ size standards (Thermo Fisher Scientific, Newington, USA) to ensure accurate results. The non-filtered sample from the dissolution test was directly added to the cell without any further preparation. Particle size measurement was initiated immediately after sample addition.

Table 3
Amount of seed crystals added to dissolution vessels.

Dissolution vessel number	Seed crystals	Amount (mg)
1	Control	0
2	Form I	1
3	Form I	4
4	Form I	7
5	Form II	1
6	Form II	4
7	Form II	7

2.9. Zeta potential determination

The surface charge properties of the non-filtration sample withdraw from non-sink dissolution testing were determined from their zeta potential values. The values were measured with a Zetasizer Nano Series from Malvern Instruments (Malvern Instruments, Malvern, UK) using a clear zeta potential cell at 25 °C.

2.10. Polarized light microscope (PLM)

The morphology of the crystal form precipitated from non-sink dissolution testing with 0 mg, Form I 7 mg, and Form II 7 mg was observed by an Axio Scope. A1 PLM (Zeiss, Oberkochen, Germany). The non-filtration samples from non-sink dissolution testing at 2 h and 5 h were dropwise on sliding glass. The polarized light birefringence cross of the samples was observed under the PLM. The images were obtained by the AxioVision Release 4.8.2 SP2 of Zeiss.

2.11. Fourier transform infrared (FTIR)

The intermolecular interactions among different crystal forms were analyzed by Fourier transform infrared (FTIR) spectra. The data were recorded by a Nicolet 6700 Fourier-Transform Infrared Spectroscopy spectrometer (Thermo Scientific, Waltham, MA, USA) using a Potassium Bromide pellets technique within the wave number range of 4000 to 500 cm^{-1} at a resolution of 2 cm^{-1}.

2.12. Scanning electron microscopy (SEM)

After being placed on a matrix and sputtered with gold, the structure and morphology of Form I, Form II, and the milled extrudes of F1 and F2 were manifested by field emission scanning electron microscopy (SEM, Thermo Fisher Scientific FIB-SEM GX4, 5KV).

2.13. Differential scanning calorimetry (DSC)

The thermal properties of Form I and Form II raw materials, tablets, and precipitates from the dissolution testing were measured using differential scanning calorimeters (DSC) (Discovery, TA Instruments, New Castle, DE, USA) equipped with refrigeration. Calibration of temperature and enthalpy was performed using indium as a standard. 4 ± 0.5 mg of each sample was weighed accurately on an analytical balance (MSA6–6S, Sartorius, Goettingen, GE) and placed in a hermetically sealed aluminum pan with a pinhole. The samples were equilibrated at 0 °C in the sample pan. The DSC curves were recorded by heating the samples at a rate of 10 °C/min from 0 °C to 180 °C in a dry nitrogen atmosphere. The data were analyzed using the TRIOS software of TA Instruments.

2.14. Powder X-ray diffraction (PXRD)

To determine the physical states of Form I, Form II, tablets, and precipitates of non-sink dissolution testing, PXRD of the samples was studied using an Ultima IV X-ray diffractometer (Rigaku Japan) with CuKα radiation (1.541836 Å) at room temperature. As samples were prepared for analysis, scraped powders or ground tablets were placed on glass sample holders and then pressed to provide smooth and uniform surfaces. Diffraction patterns were measured using a tube voltage of 40 kV and a current of 40 mA. The divergence slit and anti-scattering slit settings were set at 0.5° for the illumination on the 10 mm sample size. Scans were performed between 3° and 40° in 2θ with steps of 0.02° and a

count time of 0.1 s per step.

2.15. Statistical analysis

Triplicates of every experiment were performed. Means and standard deviations were used in expressing data. Data analysis and graphing were undertaken using OriginPro 9.0 (OriginLab Corporation, Northampton, MA, USA).

3. Results

3.1. Characterization of ritonavir Form I and II

Though there have been several excellent studies on the properties of Form I and II, some basic studies were primarily undertaken to ensure the characteristics of the two crystal forms as seed crystals or APIs (Bauer et al., 2001; Chemburkar et al., 2000; Morissette et al., 2003; Wang et al., 2021). The two crystal forms were characterized by PXRD, DSC, and FTIR. The PXRD spectrum of Form I and II was presented in Fig. 2A. The identity of the two crystal forms was established by distinguishing peaks at 6.8, 8.4, and 24.5 2-theta for Form I and 9.5, 9.8, 16.1, and 22.2 2-theta for Form II, as reported in the literature (Chemburkar et al., 2000; Miller et al., 2005). The DSC thermogram of Form I and II was shown in Fig. 2B. There was an approximately 2 °C higher melting point for Form II (approximately 123.72 °C) versus Form I (approximately 122.05 °C). The enthalpy for Form II (93.6 J/g) was greater than for Form I (72.4 J/g). The peak temperature of the melting range for Form II was approximately 3 °C higher than that of Form I. These observations accorded well with the description of the literature (Chemburkar et al., 2000; Siriwannakij et al., 2021). As shown in Fig. 2C, the FTIR spectra of Form I and II had distinctive patterns. The characteristic peaks of Form I at 3357 cm^{-1} (NH stretching of secondary amine), 2964 cm^{-1} (hydrogen-bonded acid within the molecules), 1716 cm^{-1} (C = O of carbamate), and 1644, 1622, and 1526 cm^{-1} (C = C stretching of aromatic carbons) were in agreement with the structure reported in the literature (Siriwannakij et al., 2021). While Form II was missing the peaks at 3357 cm^{-1} and the characteristic peak of hydrogen-bonded acid within the molecules, C = O of carbamate, C = C stretching of aromatic carbons shifted to 2959 cm^{-1}, 1704 cm^{-1} and 1660, 1611, and 1537 cm^{-1}, respectively.

We have tested sink dissolution under multiple pH conditions and compared the solubility of the two forms in the present study. The saturation solubility of Form I and II were determined in solutions of different pH values at 37 °C. The pH-solubility profile was presented in Fig. 2D. Form I and II exhibited a marked pH-dependent solubility profile which was similar to the trend observed by previous studies (Law et al., 2001; Rodriguez-Spong et al., 2008; Siriwannakij et al., 2021; Xu et al., 2018).

3.2. Properties of ritonavir tablets

In the present study, we were interested in developing formulations prepared via hot-melt extrusion to match the marketed product RLD Tablet, 100 mg. The F1 was prepared from Form I, while F2 was from Form II. The quality control comparison between prepared tablets and RLD was shown in the Table S2. Meanwhile, amorphous testing was performed to ensure that the tablets remained physically stable in the amorphous state. The surfaces of Form I, Form II, and the milled extrudes of F1 and F2 were characterized using SEM (Fig. 3). It has previously been observed that the initial shape of Form I particles was rods, whereas Form II appears as fine needles (Chemburkar et al., 2000). After the hot melt extrusion process and milling, the shape of the milled extrudes of F1 and F2 became blocky, and the surface seemed smooth. The morphological change of the particles resulted from high temperature, shear forces, and milling. It was evident that Form I and II disappeared to transform into amorphous forms in the milled extrudates.

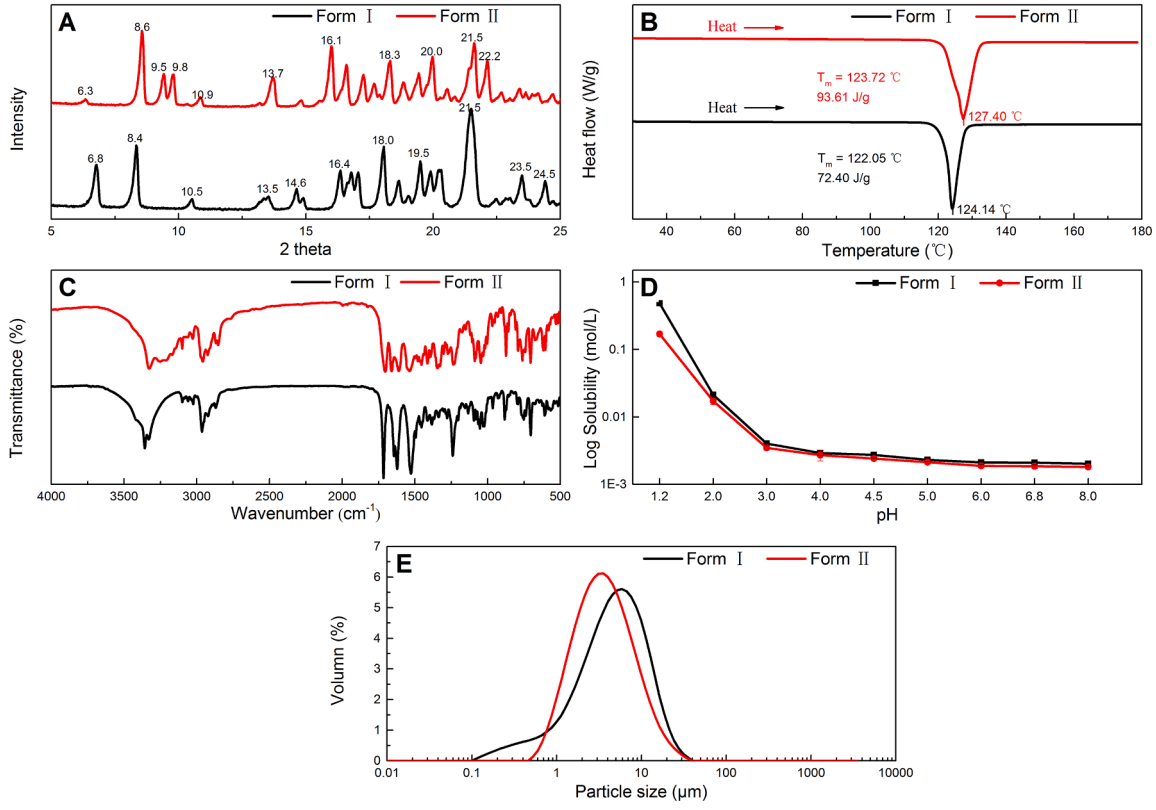

Fig. 2. Powder X-ray diffraction (PXRD) (A), Differential scanning calorimetry (DSC) (B), Fourier transform infrared (FTIR) (C), solubility at different pH values (D) of the crystalline Form I and II.

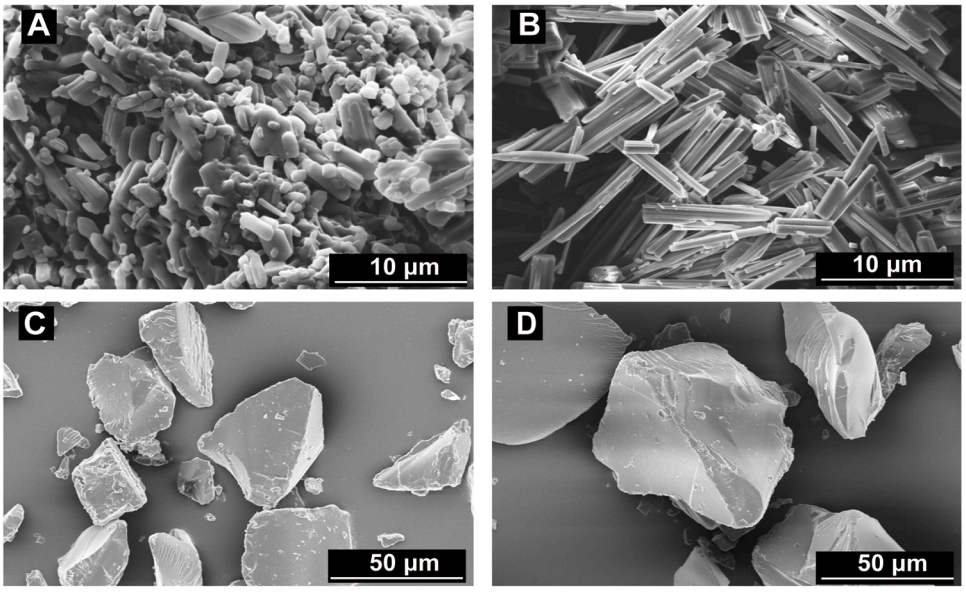

Fig. 3. Scanning electron microscopy (SEM) of Form I (A), Form II (B), milled extrudes of F1 (C), and milled extrudes of F2 (D). F1: Formulation 1; F2: Formulation 2.

PXRD patterns of the RLD, F1, and F2 tablets prepared by hot-melt extrusion did not show characteristic powder diffraction peaks but instead displayed a diffuse halo with two peaks at low 2θ values (Fig. 4A). For the tablets, PXRD diffraction showed no sharp peaks, indicating that a three-dimensional long-range order did not exist. DSC scans of the RLD, F1, and F2 tablets showed no crystallization of the drug was observed in the tablets, as there were no endotherms that may be attributed to the presence of the crystalline drug (Fig. 4B).

3.3. Dissolution testing

Fig. 5 showed the dissolution of ritonavir released from RLD, F1, and F2 in the 0.1 M hydrochloric acid (pH 1.2), water with 0.06 M polyoxyethylene 10 lauryl ether, the acetate buffer with 0.06 M polyoxyethylene 10 lauryl ether (pH 4.5), and the phosphate buffer with 0.06 M polyoxyethylene 10 lauryl ether (pH 6.8), respectively. The similarity factor f_2 of dissolution profiles of F1 and F2 compared with RLD were listed in Table 4. According to the FDA and EMA guidelines, the f_2 values between 50 and 100 suggest similar dissolution profiles (EMA, 2018; FDA, 1997). Therefore, F1 and F2 were similar to RLD in the sink conditions, which were considered suitable for testing release kinetics in the quality control context.

In the previous studies, the HME processing conditions were adjusted to vary the residual crystallinity in the resulting ASDs, thereby simulating the conditions for the incorporation of seed crystals during processing (Moseson et al., 2021, 2020). In the study, to research the effect of different seed crystals on the precipitation process of supersaturated solution, the seed crystals were added to the dissolution vessel after one hour of dissolution. The solubility of Form I and II was 3.9 μg/ml and 2.7 μg/ml in water, respectively. In comparison, the complete dissolution concentration of 100 mg ritonavir tablets was 111.1 μg/ml in 900 ml aqueous medium, thus indicating high supersaturation. The ritonavir tablets dispersed in water formed a slightly turbid dispersion. The results of the non-sink dissolution testing added with seed crystals were given in Fig. 6, where sub-Fig. A, B, and C refer to dissolution testing of RLD, F1, and F2, respectively. Though the sink dissolution testing of the formulations was conducted for 2 h, the non-sink dissolution testing was continued for 5 h in water to measure the duration of supersaturation. As shown in Table 4, the similarity factor f_2 of F1 and F2 compared to RLD were 82.1 and 80.7, respectively, which can be considered similar in dissolution profiles of water without seed crystals. The maximum drug concentration of RLD, F1 and F2 in the dissolution medium was reached within 60 min and remained in the range of more than 90% for the next 180 min. The precipitates were generated slowly from the supersaturated solution after 180 min. However, the discriminating precipitation trends were shown in dissolution profiles of RLD, F1, and F2 in the non-sink dissolution seeded with Form I and II. Dissolution profiles of tablets in the dissolution vessels not added seed crystals were marked as "n.a.". As shown in Fig. 6A, the precipitation rates of RLD were as follows: Form I 7 mg > Form I 4 mg > Form II 7 mg

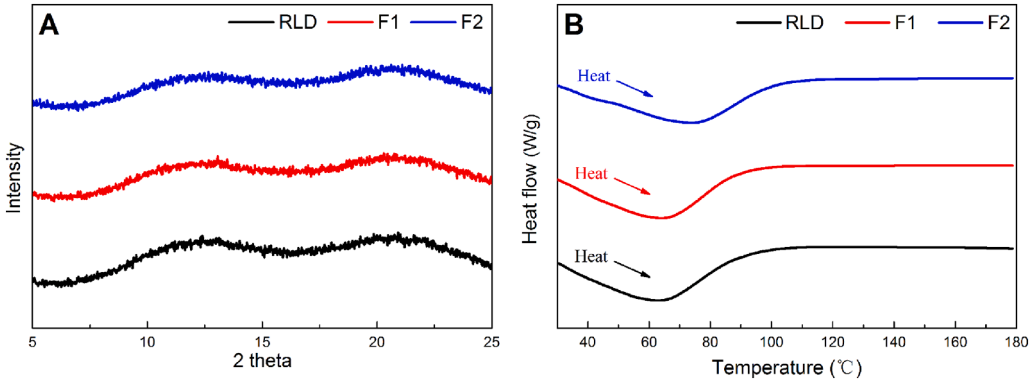

Fig. 4. PXRD (A) and DSC spectroscopy (B) of the Reference listed drug (RLD), Formulation 1 (F1), and Formulation 2 (F2).

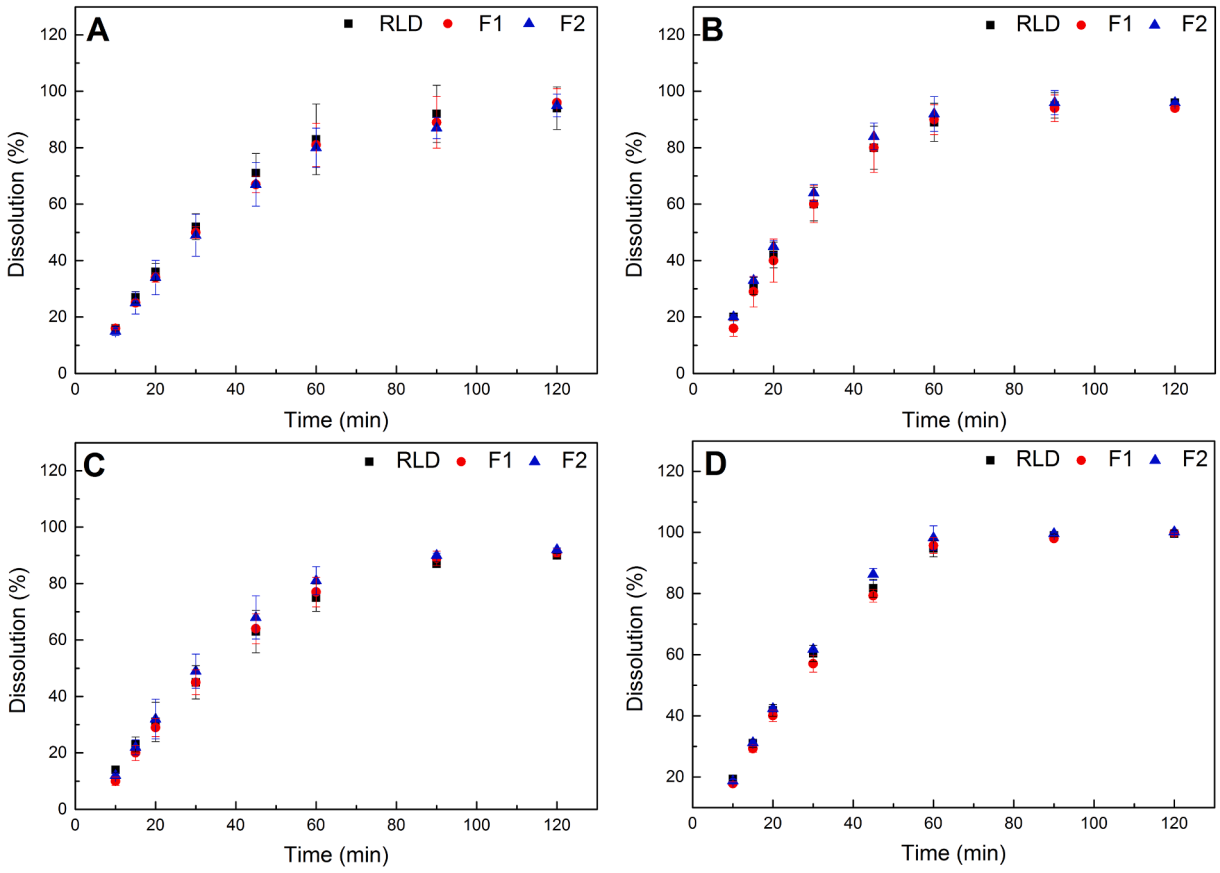

Fig. 5. Comparison of dissolution profiles of Reference listed drug (RLD), Formulation 1 (F1), and Formulation 2 (F2) in the water with 0.06 M polyoxyethylene 10 lauryl ether (A), 0.1 M hydrochloric acid (B), the phosphate buffer with 0.06 M polyoxyethylene 10 lauryl ether (C), and the acetate buffer with 0.06 M polyoxyethylene 10 lauryl ether (D), respectively. (mean ± SD, n= 3).

Table 4
The similarity factor f_2 of dissolution profiles of F1 and F2 compared with RLD.

Dissolution medium	F1	F2
0.1 M hydrochloric acid (pH 1.2)	81.8	78.1
water with 0.06 M polyoxyethylene 10 lauryl ether (USP)	82.2	75.4
acetate buffer with 0.06 M polyoxyethylene 10 lauryl ether (pH 4.5)	83.3	86.7
phosphate buffer with 0.06 M polyoxyethylene 10 lauryl ether (pH 6.8)	78.6	72.9
water	82.1	80.7

> Form II 4 mg > Form I 1 mg ≈ n.a. > Form II 1 mg. In contrast, the precipitation rate of F1 showed a different pattern: Form I 7 mg > Form I 4 mg > Form I 1 mg > Form II 7 mg > Form II 4 mg > Form II 1 mg > n.a. (Fig. 6B). Fig. 6C revealed that the precipitation behavior of F2 was similar to RLD. Although these data could not prove that Form II as API was used to prepare RLD, the supersaturated solution stability formed by the F2 prepared with Form II was more consistent with RLD than that of F1 prepared with Form I. Interestingly, the precipitation rate of supersaturated solution seeded with 1 mg of Form II was slower than that of unseeded for RLD and F2, indicating that 1 mg of Form II seeds maybe not promoting precipitation in the supersaturated solution of RLD and F2. However, the effect of seed crystals on F1 was different from that of RLD and F2. In the non-sink dissolution testing with seed crystals of F1, the precipitation rate of the supersaturated solution seeded Form II 1 mg was faster than that of unseeded for F1. 1 mg of Form I seeds had a greater effect on the precipitation rate than 7 mg of Form II seeds.

The effect of the type and amount of crystal form on the final precipitation degree of RLD, F1, and F2 were summarized in Fig. 6D. Clearly, the more seed crystals were added, the higher the degree of precipitation for the supersaturated solution of RLD, F1, and F2. As the number of seed crystals increased, the degree of precipitation among the three formulations was close. However, Form I seeds induced twice as much precipitation as Form II seeds with the same addition of 7 mg for the dissolution of the three formulations.

3.4. Particle size determination and zeta potential

The results of particle size determination and zeta potential during non-sink dissolution testing with seed crystals of ritonavir tablets are given in Fig. 7. The tablets' dissolving water was visibly turbid, which indicates the formation of light scattering species. Size determination of the solution obtained after the dissolution of RLD, F1, and F2 tablets revealed the presence of nanodroplets with a size of about 200 nm (Z-average). The particle size of the dispersed phase produced by the tablets in the dissolution medium seeded with Form I 1 mg, Form II 1 mg, and Form II 4 mg were consistent with those without seed crystals. However, in the case of the dissolution medium seeded with Form I 4 mg, Form I 7 mg, and Form II 7 mg, the particle size in the dispersion medium was ≈ 200 nm and > 4000 nm. Because the reproducibility of larger particles was poor, it was difficult to obtain reliable results. Therefore, the proportions of the two-particle sizes were not shown. According to the study conducted by Frawley et al., the presence of seed crystals in a supersaturated solution can result in a bimodal particle size distribution of the product crystals, indicating either a primary or secondary nucleation event (Frawley et al., 2012). Compared with dissolution testing in Fig. 6, it was evident that there was a steep decline in drug concentration of tablets seeded with Form I 4 mg, Form I 7 mg, and Form II 7 mg. During this time, the phase-separated drug might have partially converted from an amorphous liquid to a crystallized solid.

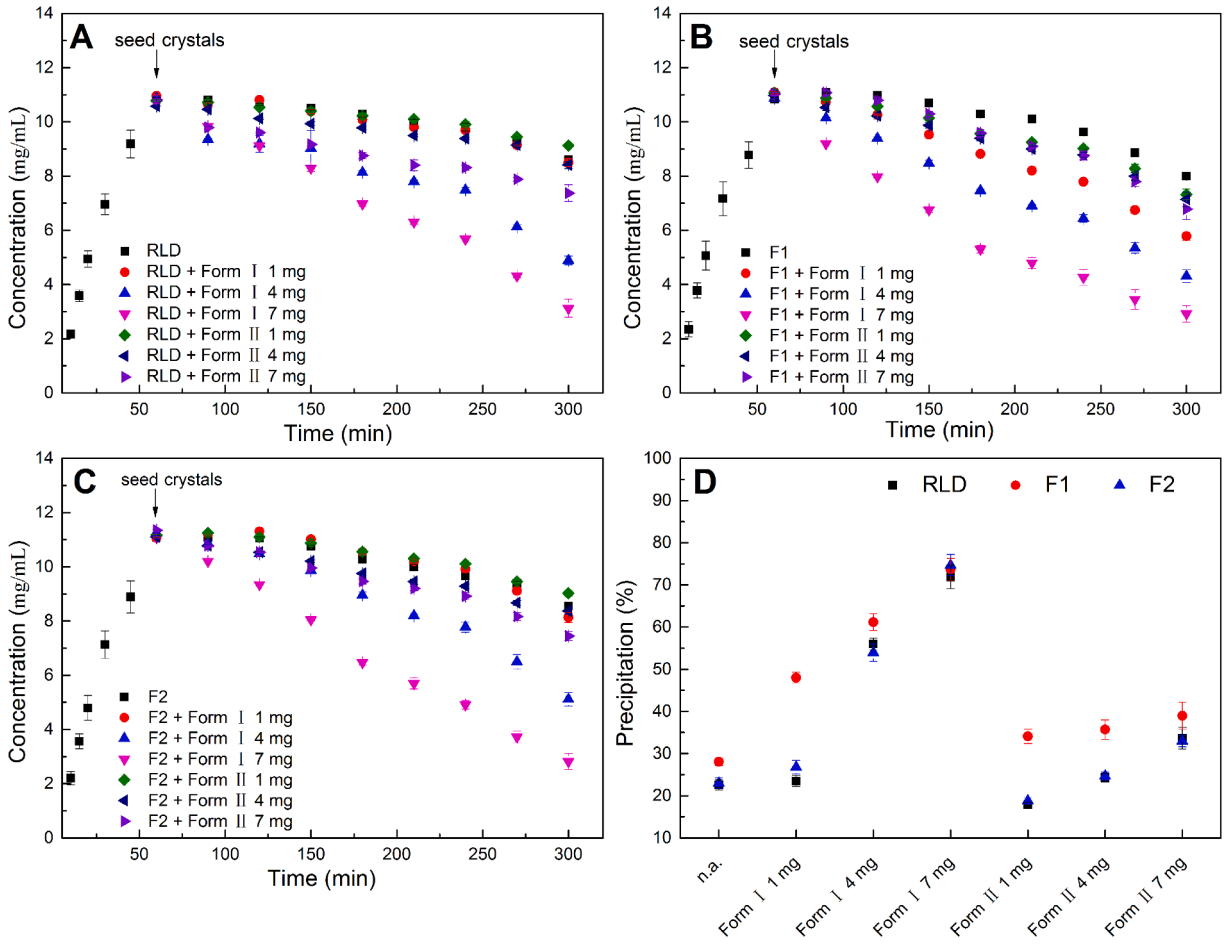

Fig. 6. Comparison of the non-sink dissolution profiles added with seed crystals of RLD (A), F1 (B), and F2 (C). The precipitation degree of RLD, F1, and F2 at 300 min (D). Dissolution profiles of tablets in the dissolution vessels not added seed crystals were marked as "n.a.". (mean ± SD, n= 3). RLD: Reference listed drug; F1: Formulation 1; F2: Formulation 2.

Therefore, the colloidal stability was assessed by zeta potential (Bhattacharjee, 2016). According to drug delivery literature, nanoparticles dispersions with zeta potential values of ± 0–10 mV, ± 10–20 mV, ± 20–30 mV, and > ± 30 mV are considered highly unstable, relatively stable, moderately stable, and highly stable, respectively (Clogston and Patri, 2011; Patel and Agrawal, 2011). As shown in Fig. 7, whether the dispersed phase in the dissolution medium was produced by RLD, F1, F2, or by adding seed crystals, the zeta potential of the supersaturated solution was maintained at −20 mV to −30 mV.

3.5. Polarized light microscope observation

Crystal morphology differences between Forms I and II were observed using PLM before confirming any changes in crystal morphology during crystal growth in the supersaturated solution (Fig. 8). Form I crystals appeared as blocks, while Form II crystals appeared as needles, as previously reported (Chemburkar et al., 2000). To further investigate the crystal growth in the supersaturated solution, The crystal morphology in unfiltered supersaturated solution from dissolution vessels at 120 min and 300 min was observed under the PLM (Fig. 9). The absence of birefringence under the PLM indicated the amorphous nature of the unfiltered supersaturated solution of RLD at 120 min (Fig. 9A). However, fine needle crystal morphology appeared at 300 min (Fig. 9D). For the supersaturated solution of RLD seeded with 7 mg of Form I, the fine needle-like crystal morphology appeared dispersed at 120 min, developing into a large radial crystal at 300 min (Fig. 9B and 9E). However, needle-like crystal morphology appeared with aggregation in the unfiltered supersaturated solution of RLD seeded with 7 mg of Form II at 120 min. The needle-like aggregates grew larger at 300 min (Fig. 9C and 9F).

Similar observations were made for unfiltered supersaturated solutions of F1 at 120 min and 300 min under PLM (Fig. 9G and 9J). The crystallization of the unfiltered supersaturated solution of F1 seeded with 7 mg of Form II was also consistent with that of RLD seeded with 7 mg of Form II at 120 min and 300 min (Fig. 9I and 9L). However, radial crystal morphology emerged at 120 min in the unfiltered supersaturated solution of F1 seeded with 7 mg of Form I, and the radial-like aggregates grew larger at 300 min (Fig. 9H and 9K). Although the PLM pattern of unfiltered supersaturated solutions of F2 was consistent with that of RLD, two kinds of crystal morphology, needle-like and radial-like, were observed in the unfiltered supersaturated solution of F2 seeded with 7 mg of Form I at 300 min (Fig. 9Q). Therefore, two types of crystals may be present in the precipitates. This phenomenon will be investigated in the next section on the physical forms of the precipitates."

3.6. Physical forms of precipitates

Solid-state properties of the precipitates were determined using DSC and PXRD analysis at the end of non-sink dissolution testing after vacuum filtration and drying. It may be observed from DSC scans in Fig. 10A–C that precipitates could be crystalline ritonavir. Furthermore, the enthalpy value increased gradually with the number of seed crystals added to the water medium, which indicated that the proportion of crystalline ritonavir was getting higher in the precipitates. It was

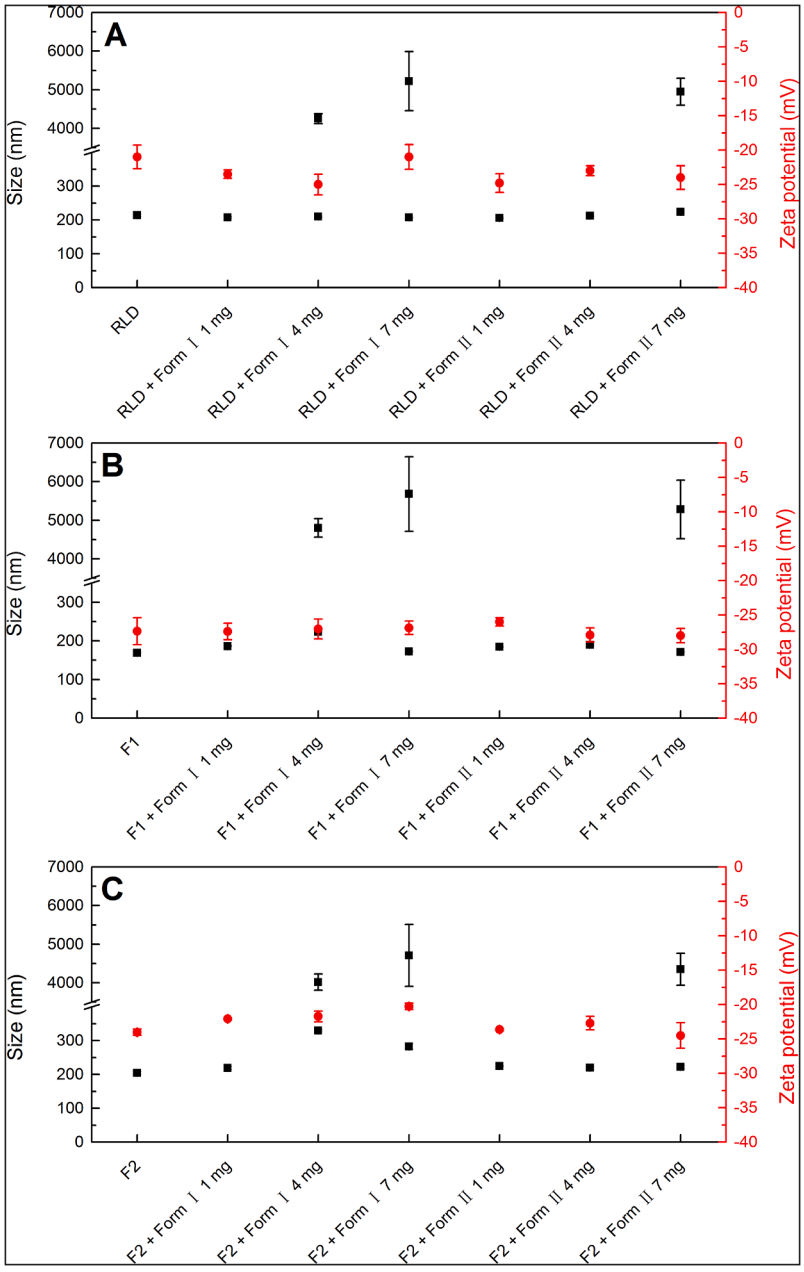

Fig. 7. Particle size determination and zeta potential during non-sink dissolution testing with seed crystals of RLD (A), F1 (B), and F2 (C). (mean ± SD, n= 3). The black square is for particle size determination, and the red circle symbols is for zeta potential. The two particle sizes of supersaturated solution seeded with Form I 4 mg, Form I 7 mg, and Form II 7 mg were reflected simultaneously in the figure, since the particle size distribution exhibited a bimodal by the dynamic light scattering (DLS). RLD: Reference listed drug; F1: Formulation 1; F2: Formulation 2.

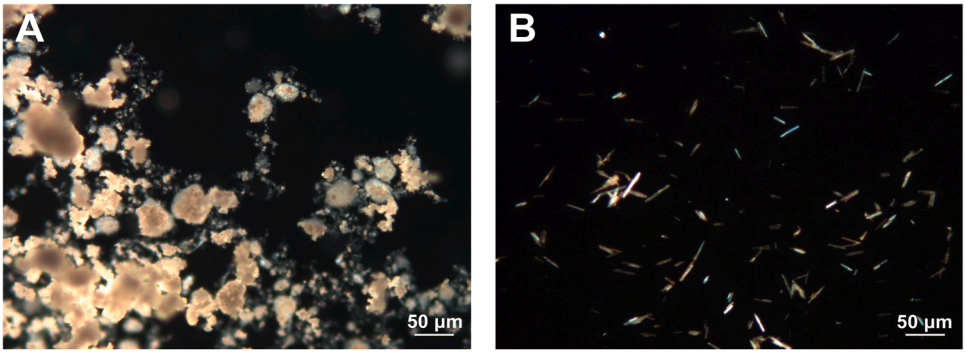

Fig. 8. Polarized light microscope (PLM) of the crystalline Form I (A) and Form II (B).

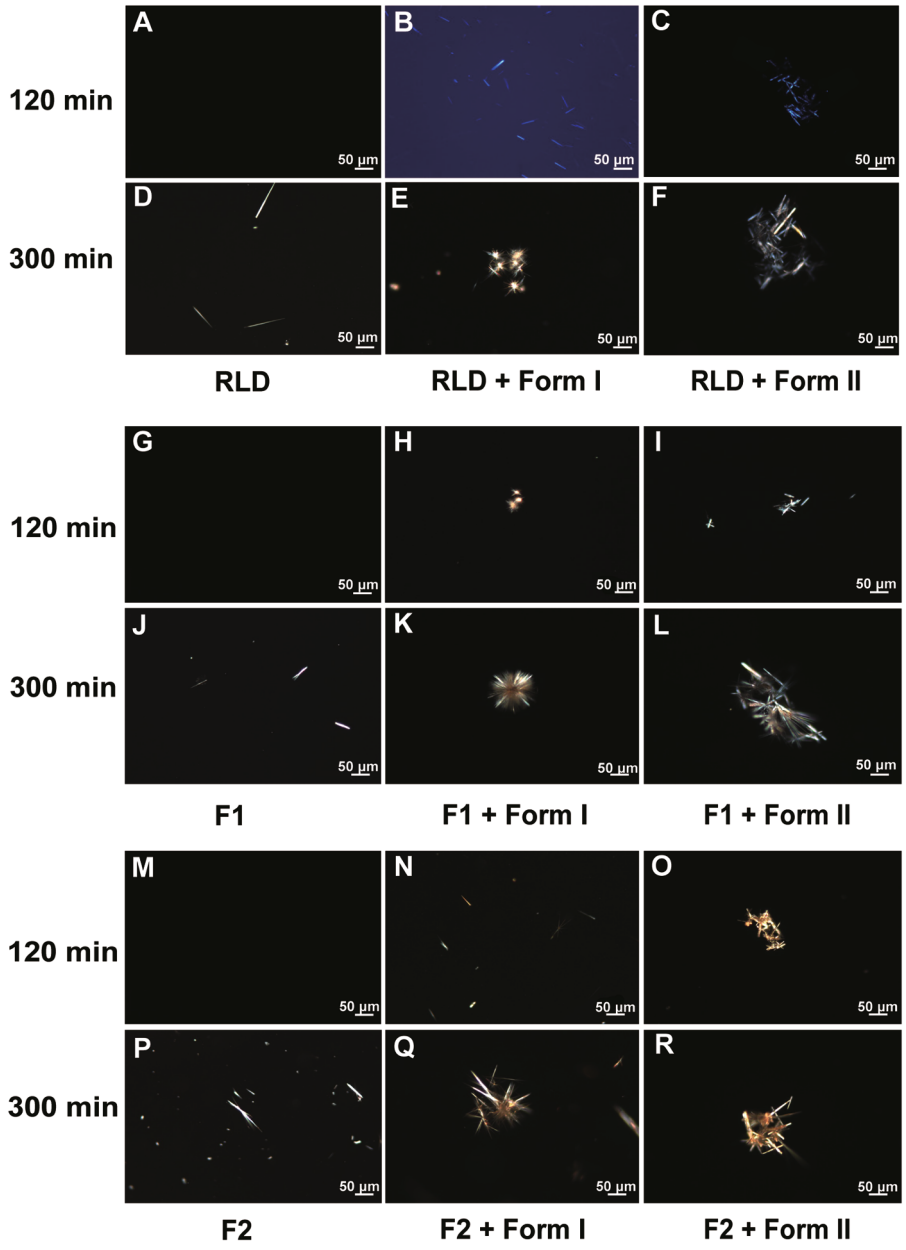

Fig. 9. PLM of unfiltered supersaturated solution from dissolution vessels with 0 mg, Form I 7 mg, and Form II 7 mg at 120 min and 300 min of RLD (A–F), F1 (G–L), and F2 (M–R). RLD: Reference listed drug; F1: Formulation 1; F2: Formulation 2.

possible to predict the DSC thermogram of precipitates from the dissolution test results of non-sink dissolution testing with seed crystals presented earlier in Fig. 6, which showed a dramatic decrease in drug concentration, indicating the recrystallization of ritonavir. Moreover, the enthalpy of the precipitates from non-sink dissolution testing seeded with Form II 1 mg of RLD and F2 was lower than that of the unseeded. In contrast, the enthalpy of the precipitates from non-sink dissolution testing seeded with Form II 1 mg of F1 was higher than that of the unseeded, which corresponds to the dissolution profile in Fig. 6.

Fig. 10D–F showed PXRD patterns that support DSC results. The precipitates exhibited characteristic peaks of crystalline ritonavir. The area of characteristic peaks increased gradually with the increase of the amount of seed crystals added to the non-sink dissolution testing. The crystalline form of precipitates could be known by comparing the characteristic peaks of Form I and II in Fig. 2A. The precipitates obtained from non-sink dissolution testing without seed crystals of RLD, F1, and F2 were Form I. The results showed that as the amount of Form I seeds increased, the characteristic peak of Form II, especially at 9.5 2-theta, became more prominent in the precipitates from the non-sink dissolution test of RLD and F2, as shown in Fig. 10D and 10F. However, Form I did not have this effect on the precipitates from the non-sink dissolution test of F1, as shown in Fig. 10E. On the other hand, as the amount of Form II seeds increased, the characteristic peak of Form I became less prominent in the precipitates from the non-sink dissolution test of RLD, F1, and F2.

4. Discussion

HME technology is attractive for the commercial production of ASDs since it provides rapid formulation development and scale-up process. Despite the high standards in pharmaceutical industry, there may still be potential for contamination of the amorphous formulation by seed crystals in the HME manufacturing process. This contamination mostly leads to the precipitation of supersaturated solutions formed by ASD.

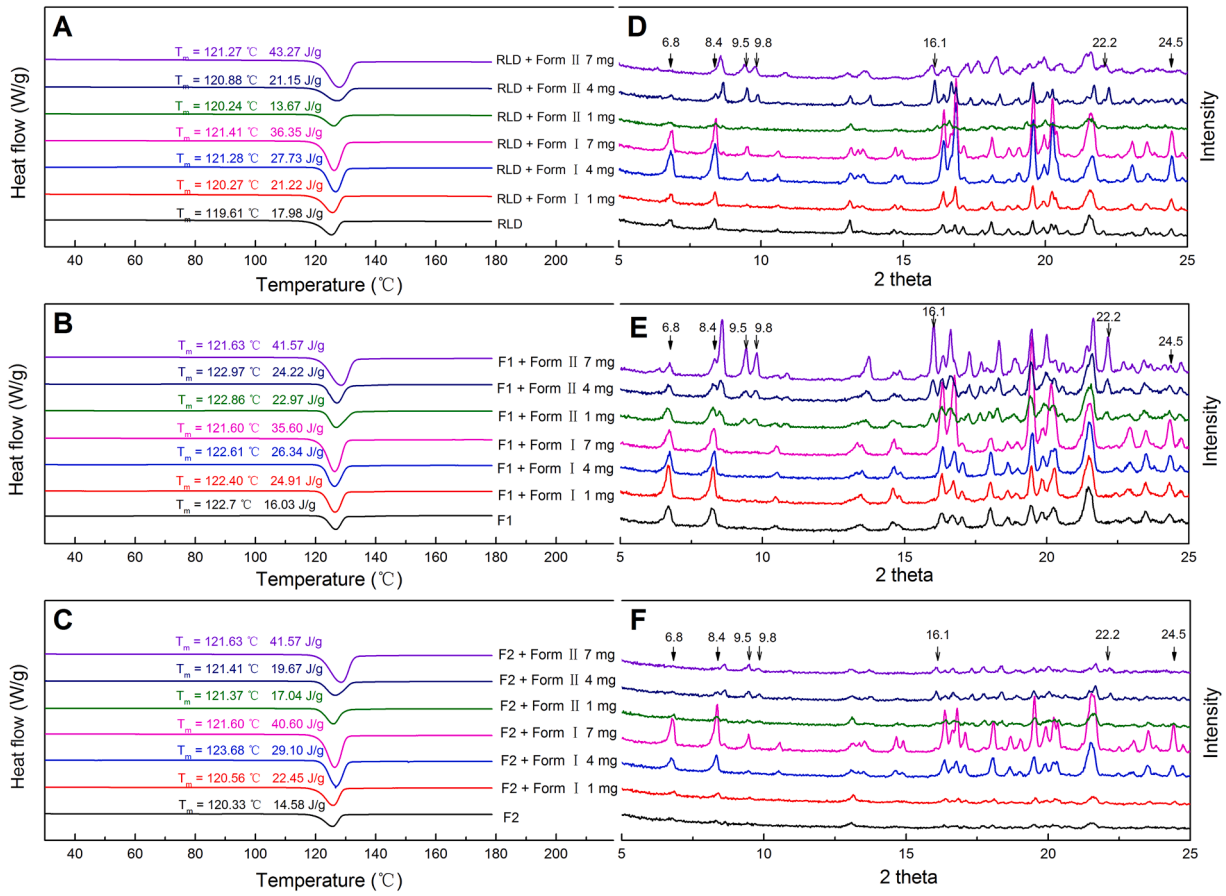

Fig. 10. DSC thermogram of precipitates obtained from non-sink dissolution testing with seed crystals of RLD (A), F1 (B), and F2 (C). PXRD patterns of precipitates obtained from non-sink dissolution testing with seed crystals of RLD (D), F1 (E), and F2 (F). RLD: Reference listed drug; F1: Formulation 1; F2: Formulation 2.

The introduction of seed crystals can occur through improper process parameters during HME leading to seed residues, or due to mechanical stress during grinding and tableting which may compromise the amorphous state of the drug substance. These factors may impact the transformation of the crystalline drug into an amorphous form (Hanada et al., 2018; Ma et al., 2019; Pas et al., 2020). In this study, ritonavir was chosen as the model compound with a relatively slow crystallization tendency (Baird et al., 2010). Ritonavir is a polymorphic drug with metastable Form I and stable Form II. Form II has higher conformational deformation, lattice, and surface energies relative to Form I, consisting with its lower solubility and bioavailability (Wang et al., 2021). According to Ostwald's rule of stages, solution-mediated polymorphic transitions are controlled by the difference in solubility between stable and metastable crystals (Iohara et al., 2019). In addition, one of the challenges in formulating ritonavir as a drug product is its low solubility, which can limit its bioavailability and therapeutic efficacy. Furthermore, ritonavir tends to form amorphous or poorly crystalline solids, which can adversely affect the stability and performance of the drug product. These characteristics of ritonavir can make its formulation and manufacture difficult, and can lead to problems such as poor dissolution and bioavailability, inadequate shelf-life, and variable pharmacokinetics. As a result, understanding and improving the crystallization behavior of ritonavir is an important area of research for the pharmaceutical industry. This makes it a useful test case for evaluating the efficacy of new approaches for improving the crystallization of drug substances. If the approach was successful in improving the crystallization of ritonavir, it could potentially be applied to other poorly crystallizing drugs, including fast crystallizers.

Water rather than simulated biological fluid was selected as the medium to study the effect of different seed crystals on the precipitation process of supersaturated solution during the non-sink dissolution test. Therefore, it is possible that the results of this study may not fully reflect the behavior of ritonavir in the human body, particularly with regards to its oral bioavailability. However, the use of water as the non-sink dissolution medium provided a more challenging environment for ritonavir to precipitation, so we can better understand the supersaturated behaviors of the system. Based on the data in Fig. 6, the dissolution behavior of RLD, F1, and F2 was similar in the non-sink dissolution without seed crystals in four hours. However, the final precipitation degree of F1 was higher than that of RLD and F2. This indicated a difference in the stability of the supersaturated solutions formed by ASD prepared from two crystal forms. At the same time, the crystal forms precipitated from supersaturated solutions without seed crystals of these three formulations were all Form I (Fig. 10). The phenomenon was consistent with previous studies that ritonavir (Form I or II) only crystallized as Form I or an amorphous material under different recrystallization conditions in various solvent systems (Chemburkar et al., 2000). According to Ostwald rule, the less stable form precipitates first and crystallizes more easily and preferably. However, the precipitation rate of F1 was faster than that of RLD and F2 in the non-sink dissolution testing seeded Form I (Fig. 6A–C). Interestingly, when the amount of seed Form I was increased gradually in the supersaturated solution of these three formulations, Form II appeared and increased in the precipitates of RLD and F2 (Fig. 10D and 10F), but not that of F1 (Fig. 10E). The transformation pathways were consistent with the previous study: amorphous > lyotropic liquid crystalline >> Form *I* > Form II (Rodriguez-Spong et al., 2008). However, unless highly supersaturated solutions are present, the conversion of Form I to Form II is energetically unfavorable in the dosage form development (Bauer et al., 2001). Since all three formulations have similar levels of supersaturation, it is

possible that the reason for the appearance of Form II in the RLD and F2 precipitates was that the RLD and F2 themselves had trace seeds of Form II that cannot be detected by PXRD and DSC. The experiment of adding seed crystal Form II could also imply that F1 itself had trace seeds of Form I. These results demonstrated that Form I lead to more precipitation than Form II.

As described above, Ma et al. and Hanada et al. found that the conversion of the crystalline drug into an amorphous form is affected by mechanical and thermal energy inputs in the HME (Hanada et al., 2018; Ma et al., 2019). The material degrades during preparation if the mechanical and thermal energy are too high. On the contrary, if the mechanical and thermal energy are too low, the material cannot be free of crystalline drug particles and mixed uniformly. Ideally, either form of ritonavir would be converted to amorphous by HME. However, lower mechanical and thermal energy inputs may be selected to prevent excessive product degradation that may lead to small crystalline domains within the formulation. It can be noted that seeded 1 mg of Form II to the supersaturated solution formed by RLD and F2 not only did not lead to more precipitation but instead helped to maintain the stability of the supersaturated solution. Although HME transformed both Form I and Form II into amorphous form in the ASD and showed that they exhibit similar dissolution profiles as that of the RLD, seeded 1 mg of Form I to the supersaturated solution formed by F1 did not achieve the function of maintaining supersaturation. This suggests that higher mechanical and thermal energy inputs are required for the formulation prepared by Form I to ensure the complete conversion of crystalline drug to amorphous. There is no clear explanation for the difference between the effects of the two seed crystals in the formulation. The next section of the survey was concerned with the reason for this phenomenon through PLM observations.

Observing the precipitates in a sample through PLM provided a means to detect changes in particle size and shape over time. Unfiltered supersaturated solutions of the three formulations seeded with Form I 4 mg, Form I 7 mg, and Form II 7 mg observed under PLM were consistent with the results of particle size determination (Fig. 9). Based on the images, it appears that the precipitates at the 120 min were in the submicron range, while the particles at the 300 min seem to be in the micron range. In supersaturated solutions, as new precipitates crystallize, they interact with existing crystals, leading to crystal growth and increased particle size of the precipitate. Mechanistically, nucleation and crystal growth are the two primary processes involved in drug precipitation from a supersaturated solution (Brouwers et al., 2009). Nucleation must form before it can become crystal growth. Anwar et al. revealed the formation of molecular aggregates in solution that nucleate to form crystals upon contact with the seed surface (Anwar et al., 2015). The new crystallites are weakly bound to the crystal surface and can be easily sheared by fluid, making the seed surfaces accessible again. We observed the crystal growth process of Form I and Form II in the supersaturated solution formed by RLD (Fig. 9A–F). Although the crystal morphology of both forms exhibits needle-like/lath-like characteristics with faster-growing hydrophobic sides and slower-growing hydrophilic capping faces (Wang et al., 2021), Form II was always the needle-like aggregation in the supersaturated solution (Fig. 9C and 9F). On the other hand, Form I was initially formed as fine needles dispersed in solution (Fig. 9B) and finally aggregated into a radial crystal morphology (Fig. 9E). Therefore, Form I precipitated from supersaturated solution was dispersed in the solution, easily sheared by fluid, and in turn, served as seeds. The difference in the dispersion state of Form I and Form II in supersaturated solution may be related to their physical-chemical properties. According to the classical nucleation theory (CNT), which achieves the near-equilibrium state through crystallization on a single barrier, the nucleation rate strongly depends on supersaturation and the interfacial energy between the critical cluster and the solvent (Anisimova et al., 2005; Brouwers et al., 2009; Zhang et al., 2021). Therefore, Form II may have higher interface energy per unit area relative to Form I, which is consistent with its slower crystal growth in supersaturated solutions formed by ASD. This could be why Form I had a more negative impact than Form II on the stability of the supersaturated solutions formed by ASD.

5. Conclusions

The study successfully developed ritonavir tablets using the HME process with both Form I and II polymorphs, which demonstrated similar dissolution profiles to RLD. The investigation revealed that the metastable Form I was the preferred polymorph to precipitate without seed crystals. However, the presence of seed crystals had a significant impact on the supersaturation stabilization of the amorphous formulation. The results showed that the presence of seed crystals, particularly the metastable Form I seed, had a negative impact on the supersaturation stabilization of the amorphous formulation, leading to more precipitation compared to the stable Form II seed. The Form I crystals that precipitated from the supersaturated solution were easily dispersed in the solution and could serve as seeds to facilitate crystal growth, while Form II crystals tended to grow more slowly and presented as aggregates.

The study further revealed that the precipitation of Form I from supersaturated solution was somewhat inhibited by Form II seeds, suggesting that the presence of Form II seeds could be beneficial in preventing the growth of undesirable crystals of Form I. These findings highlight the importance of minimizing the contamination risk of seed crystals during the HME manufacturing process and selecting the appropriate polymorph for the production of ASDs. In conclusion, the investigation also provides insights into the existence of drug crystals that facilitate the crystal growth of the drug in the supersaturated solutions formed by ASD, which can affect the solubility and absorption of the drug. This study can be useful as a model for selecting crystal forms in the development of other polymorphic drugs for ASD.

Funding

This work is financially supported by the National Science and Technology Major Project (no. 2017ZX09201–003), the Open Project of Shandong Collaborative Innovation Center for Antibody Drugs (No. CICAD1828), and Tai-Shan Scholar Research Fund of Shandong Province of China.

Credit authorship contribution statement

All authors read and approved the final manuscript.

CRediT authorship contribution statement

Hengqian Wu: Investigation, Methodology, Writing – original draft, Visualization, Validation. **Zhengping Wang:** Methodology, Writing – review & editing, Visualization. **Yanna Zhao:** Writing – review & editing, Software, Visualization. **Yan Gao:** Investigation, Methodology. **Lili Wang:** Methodology, Methodology. **Heng Zhang:** Investigation, Software. **Rupeng Bu:** Writing – review & editing. **Zhuang Ding:** Writing – review & editing. **Jun Han:** Conceptualization, Resources, Writing – review & editing, Supervision.

Declaration of Competing Interest

The authors declare that there are no competing financial interests. Zhengping Wang and Jun Han are the employee of the Liaocheng High-Tech Biotechnology Co., Ltd. The company had no role in the design of the study; in the collection, analyses, or interpretation of data; in the writing of the manuscript, and in the decision to publish the results.

Data availability

Data will be made available on request.

Acknowledgments

We thank the Research and Development group of Liaocheng High-Tech Biotechnology Co., Ltd. for excellent technical assistance. The above work was also technically supported by Shandong Province Collaborative Innovation Center for Antibody Drugs, Shandong Province Engineering Research Center for Nanomedicine and Drug Delivery Systems and Shandong Province Engineering Laboratory of Anti-Viral Drugs.

Supplementary materials

Supplementary material associated with this article can be found, in the online version, at doi:10.1016/j.ejps.2023.106440.

References

Abuzar, S.M., Hyun, S.M., Kim, J.H., Park, H.J., Kim, M.S., Park, J.S., Hwang, S.J., 2018. Enhancing the solubility and bioavailability of poorly water-soluble drugs using supercritical antisolvent (SAS) process. Int. J. Pharm. 538, 1–13. https://doi.org/10.1016/j.ijpharm.2017.12.041.

Alonzo, D.E., Raina, S., Zhou, D., Gao, Y., Zhang, G.G., Taylor, L.S., 2012. Characterizing the impact of hydroxypropylmethyl cellulose on the growth and nucleation kinetics of felodipine from supersaturated solutions. Cryst. Growth Des. 12, 1538–1547. https://doi.org/10.1021/cg201590j.

Alzahrani, A., Nyavanandi, D., Mandati, P., Youssef, A.A.A., Narala, S., Bandari, S., Repka, M., 2022. A systematic and robust assessment of hot-melt extrusion-based amorphous solid dispersions: theoretical prediction to practical implementation. Int. J. Pharm. 624, 121951 https://doi.org/10.1016/j.ijpharm.2022.121951.

Amidon, G.L., Lennernäs, H., Shah, V.P., Crison, J.R., 1995. A theoretical basis for a biopharmaceutic drug classification: the correlation of in vitro drug product dissolution and in vivo bioavailability. Pharm. Res. 12, 413–420. https://doi.org/10.1023/A:1016212804288.

Anisimova, L., Anisimov, M., Semin, G., Turner, P., Hopke, P.K., 2005. An algorithm for semi-empirical design of nucleation rate surface. J. Colloid Interface Sci. 290, 107–116. https://doi.org/10.1016/j.jcis.2005.04.021.

Anwar, J., Khan, S., Lindfors, L., 2015. Secondary crystal nucleation: nuclei breeding factory uncovered. Angew. Chem. Int. Ed. 54, 14681–14684. https://doi.org/10.1002/anie.201501216.

Baird, J.A., Van Eerdenbrugh, B., Taylor, L.S., 2010. A classification system to assess the crystallization tendency of organic molecules from undercooled melts. J. Pharm. Sci. 99, 3787–3806. https://doi.org/10.1002/jps.22197.

Bauer, J., Spanton, S., Henry, R., Quick, J., Dziki, W., Porter, W., Morris, J., 2001. Ritonavir: an extraordinary example of conformational polymorphism. Pharm. Res. 18, 859–866. https://doi.org/10.1023/A:1011052932607.

Best, B.M., Capparelli, E.V., Diep, H., Rossi, S.S., Farrell, M.J., Williams, E., Lee, G., Van den Anker, J.N., Rakhmanina, N., 2011. Pharmacokinetics of lopinavir/ritonavir crushed versus whole tablets in children. J. Acquir. Immune. Defic. Syndr. 58, 385–391. https://doi.org/10.1097/QAI.0b013e318232b057.

Bhattacharjee, S., 2016. DLS and zeta potential - What they are and what they are not? J. Controlled Release 235, 337–351. https://doi.org/10.1016/j.jconrel.2016.06.017.

Brouwers, J., Brewster, M.E., Augustijns, P., 2009. Supersaturating drug delivery systems: the answer to solubility-limited oral bioavailability? J. Pharm. Sci. 98, 2549–2572. https://doi.org/10.1002/jps.21650.

Chemburkar, S.R., Bauer, J., Deming, K., Spiwek, H., Patel, K., Morris, J., Henry, R., Spanton, S., Dziki, W., Porter, W., Quick, J., Bauer, P., Donaubauer, J., Narayanan, B.A., Soldani, M., Riley, D., McFarland, K., 2000. Dealing with the impact of ritonavir polymorphs on the late stages of bulk drug process development. Org. Proc. Res. Dev. 4, 413–417. https://doi.org/10.1021/op000023y.

Choi, J.S., Kwon, S.H., Lee, S.E., Jang, W.S., Byeon, J.C., Jeong, H.M., Park, J.S., 2017. Use of acidifier and solubilizer in tadalafil solid dispersion to enhance the in vitro dissolution and oral bioavailability in rats. Int. J. Pharm. 526, 77–87. https://doi.org/10.1016/j.ijpharm.2017.04.056.

Clogston, J.D., Patri, A.K., 2011. Zeta potential measurement. Methods Mol. Biol. 697, 63–70. https://doi.org/10.1007/978-1-60327-198-1_6.

Dahan, A., Beig, A., Ioffe-Dahan, V., Agbaria, R., Miller, J.M., 2013. The twofold advantage of the amorphous form as an oral drug delivery practice for lipophilic compounds: increased apparent solubility and drug flux through the intestinal membrane. AAPS J 15, 347–353. https://doi.org/10.1208/s12248-012-9445-3.

EMA, 2018. Question and answer on the adequacy of the Mahalanobis distance to assess the comparability of drug dissolution profiles. https://www.ema.europa.eu/en/documents/scientific-guideline/question-answer-adequacy-mahalanobis-distance-assess-comparability-drug-dissolution-profiles_en.pdf.

FDA, 1997. Dissolution testing of immediate release solid oral dosage forms guidance for industry. https://www.fda.gov/downloads/drugs/guidances/ucm070237.pdf.

Fenske, D.B., Chonn, A., Cullis, P.R., 2008. Liposomal nanomedicines: an emerging field. Toxicol. Pathol. 36, 21–29. https://doi.org/10.1177/0192623307310.

Frawley, P.J., Mitchell, N.A., Ó'Ciardhá, C.T., Hutton, K.W., 2012. The effects of supersaturation, temperature, agitation and seed surface area on the secondary nucleation of paracetamol in ethanol solutions. Chem. Eng. Sci. 75, 183–197. https://doi.org/10.1016/j.ces.2012.03.041.

Goldberg, A.H., Gibaldi, M., Kanig, J.L., 1966. Increasing dissolution rates and gastrointestinal absorption of drugs via solid solutions and eutectic mixtures. IV. Chloramphenicolurea system. J. Pharm. Sci. 55, 581–583. https://doi.org/10.1002/jps.2600550610.

Guan, Q., Ma, Q., Zhao, Y., Jiang, X., Zhang, H., Liu, M., Wang, Z., Han, J., 2021. Cellulose derivatives as effective recrystallization inhibitor for ternary ritonavir solid dispersions: in vitro-in vivo evaluation. Carbohydr. Polym. 273, 118562 https://doi.org/10.1016/j.carbpol.2021.118562.

Guo, Y., Wang, C., Dun, J., Du, L., Hawley, M., Sun, C.C., 2019. Mechanism for the reduced dissolution of ritonavir tablets by sodium lauryl sulfate. J. Pharm. Sci. 108, 516–524. https://doi.org/10.1016/j.xphs.2018.10.047.

Guzmán, H.R., Tawa, M., Zhang, Z., Ratanabanangkoon, P., Shaw, P., Gardner, C.R., Chen, H., Moreau, J.P., Almarsson, Ö., Remenar, J.F., 2007. Combined use of crystalline salt forms and precipitation inhibitors to improve oral absorption of celecoxib from solid oral formulations. J. Pharm. Sci. 96, 2686–2702. https://doi.org/10.1002/jps.20906.

Hanada, M., Jermain, S.V., Lu, X., Su, Y., Williams III, R.O, 2018. Predicting physical stability of ternary amorphous solid dispersions using specific mechanical energy in a hot melt extrusion process. Int. J. Pharm. 548, 571–585. https://doi.org/10.1016/j.ijpharm.2018.07.029.

Ilevbare, G.A., Taylor, L.S., 2013. Liquid–liquid phase separation in highly supersaturated aqueous solutions of poorly water-soluble drugs: implications for solubility enhancing formulations. Cryst. Growth Des. 13, 1497–1509. https://doi.org/10.1021/cg301679h.

Iohara, D., Anraku, M., Uekama, K., Hirayama, F., 2019. Modification of drug crystallization by cyclodextrins in pre-formulation study. Chem. Pharm. Bull. 67, 915–920. https://doi.org/10.1248/cpb.c18-00752.

Jermain, S.V., Brough, C., Williams III, R.O, 2018. Amorphous solid dispersions and nanocrystal technologies for poorly water-soluble drug delivery - An update. Int. J. Pharm. 535, 379–392. https://doi.org/10.1016/j.ijpharm.2017.10.051.

Lamb, Y.N., 2022. Nirmatrelvir plus ritonavir: first approval. Drugs 82, 585–591. https://doi.org/10.1007/s40265-022-01692-5.

Law, D., Krill, S.L., Schmitt, E.A., Fort, J.J., Qiu, Y., Wang, W., Porter, W.R., 2001. Physicochemical considerations in the preparation of amorphous ritonavir-poly (ethylene glycol) 8000 solid dispersions. J. Pharm. Sci. 90, 1015–1025. https://doi.org/10.1002/jps.1054.

Law, D., Schmitt, E.A., Marsh, K.C., Everitt, E.A., Wang, W., Fort, J.J., Krill, S.L., Qiu, Y., 2004. Ritonavir-PEG 8000 amorphous solid dispersions: in vitro and in vivo evaluations. J. Pharm. Sci. 93, 563–570. https://doi.org/10.1002/jps.10566.

Li, N., Taylor, L.S., 2018. Tailoring supersaturation from amorphous solid dispersions. J. Controlled Release 279, 114–125. https://doi.org/10.1016/j.jconrel.2018.04.014.

Ma, X., Huang, S., Lowinger, M.B., Liu, X., Lu, X., Su, Y., Williams III, R.O, 2019. Influence of mechanical and thermal energy on nifedipine amorphous solid dispersions prepared by hot melt extrusion: preparation and physical stability. Int. J. Pharm. 561, 324–334. https://doi.org/10.1016/j.ijpharm.2019.03.014.

Miller, J.M., Beig, A., Carr, R.A., Spence, J.K., Dahan, A., 2012. A win-win solution in oral delivery of lipophilic drugs: supersaturation via amorphous solid dispersions increases apparent solubility without sacrifice of intestinal membrane permeability. Mol. Pharmaceutics 9, 2009–2016. https://doi.org/10.1021/mp300104s.

Miller, J.M., Collman, B.M., Greene, L.R., Grant, D.J., Blackburn, A.C., 2005. Identifying the stable polymorph early in the drug discovery-development process. Pharm. Dev. Technol. 10, 291–297. https://doi.org/10.1081/PDT-54467.

Mohammadian, M., Salami, M., Momen, S., Alavi, F., Emam-Djomeh, Z., Moosavi-Movahedi, A.A., 2019. Enhancing the aqueous solubility of curcumin at acidic condition through the complexation with whey protein nanofibrils. Food Hydrocoll 87, 902–914. https://doi.org/10.1016/j.foodhyd.2018.09.001.

Morissette, S.L., Salami, M., Momen, S., Alavi, F., Emam-Djomeh, Z., Moosavi-Movahedi, A.A., 2003. Elucidation of crystal form diversity of the HIV protease inhibitor ritonavir by high-throughput crystallization. Proc. Natl. Acad. Sci. U.S.A. 100, 2180–2184. https://doi.org/10.1073/pnas.0437744100.

Moseson, D.E., Parker, A.S., Beaudoin, S.P., Taylor, L.S., 2020. Amorphous solid dispersions containing residual crystallinity: influence of seed properties and polymer adsorption on dissolution performance. Eur. J. Pharm. Sci. 146, 105276 https://doi.org/10.1016/j.ejps.2020.105276.

Moseson, D.E., Corum, I.D., Lust, A., Altman, K.J., Hiew, T.N., Eren, A., Nagy, Z.K., Taylor, L.S., 2021. Amorphous solid dispersions containing residual crystallinity: competition between dissolution and matrix crystallization. AAPS J 23, 1–18. https://doi.org/10.1208/s12248-021-00598-6.

Pas, T., Verbert, S., Appeltans, B., Van den Mooter, G., 2020. The influence of crushing amorphous solid dispersion dosage forms on the in-vitro dissolution kinetics. Int. J. Pharm. 573, 118884 https://doi.org/10.1016/j.ijpharm.2019.118884.

Patel, V.R., Agrawal, Y.K., 2011. Nanosuspension: an approach to enhance solubility of drugs. J. Adv. Pharm. Technol. Res. 2, 81–87. https://doi.org/10.4103/2231-4040.82950.

Proietti, S., Carlomagno, G., Dinicola, S., Bizzarri, M., 2014. Soft gel capsules improve melatonin's bioavailability in humans. Expert Opin. Drug Metab. Toxicol. 10, 1193–1198. https://doi.org/10.1517/17425255.2014.943183.

Raina, S.A., Zhang, G.G., Alonzo, D.E., Wu, J., Zhu, D., Catron, N.D., Gao, Y., Taylor, L.S., 2015. Impact of solubilizing additives on supersaturation and membrane transport of drugs. Pharm. Res. 32, 3350–3364. https://doi.org/10.1007/s11095-015-1712-4.

Reggane, M., Wiest, J., Saedtler, M., Harlacher, C., Gutmann, M., Zottnick, S.H., Piechon, P., Dix, I., Buschbaum, K.M., Holzgrabe, U., Meinel, L., Galli, B., 2018. Bioinspired co-crystals of Imatinib providing enhanced kinetic solubility. Eur. J. Pharm. Biopharm. 128, 290–299. https://doi.org/10.1016/j.ejpb.2018.05.012.

Rodriguez-Spong, B., Acciacca, A., Fleisher, D., Rodriguez-Hornedo, N., 2008. PH-induced nanosegregation of ritonavir to lyotropic liquid crystal of higher solubility than crystalline polymorphs. Mol. Pharmaceutics 5, 956–967. https://doi.org/10.1021/mp800114k.

Singh, A., Van den Mooter, G., 2016. Spray drying formulation of amorphous solid dispersions. Adv. Drug Delivery Rev. 100, 27–50. https://doi.org/10.1016/j.addr.2015.12.010.

Sekiguchi, K., Obi, N., 1961. Studies on absorption of eutectic mixture. I. A comparison of the behavior of eutectic mixture of sulfathiazole and that of ordinary sulfathiazole in man. Chem. Pharm. Bull. 9, 866–872. https://doi.org/10.1248/cpb.9.866.

Serajuddin, A.T., 2007. Salt formation to improve drug solubility. Adv. Drug Delivery Rev. 59, 603–616. https://doi.org/10.1016/j.addr.2007.05.010.

Sherman, E.M., Steinberg, J.G., 2011. Heat-stable ritonavir tablets: a new formulation of a pharmacokinetic enhancer for HIV. Expert Opin. Pharmacother. 12, 141–148. https://doi.org/10.1517/14656566.2011.542151.

Siriwannakij, N., Heimbach, T., Serajuddin, A.T., 2021. Aqueous dissolution and dispersion behavior of polyvinylpyrrolidone vinyl acetate-based amorphous solid dispersion of ritonavir prepared by hot-melt extrusion with and without added surfactants. J. Pharm. Sci. 110, 1480–1494. https://doi.org/10.1016/j.xphs.2020.08.007.

Solanki, N.G., Kathawala, M., Serajuddin, A.T., 2019. Effects of surfactants on itraconazole-hydroxypropyl methylcellulose acetate succinate solid dispersion prepared by hot melt extrusion. II: rheological analysis and extrudability testing. J. Pharm. Sci. 108, 3063–3073. https://doi.org/10.1016/j.xphs.2019.09.014.

Stephenson, G.A., Aburub, A., Woods, T.A., 2011. Physical stability of salts of weak bases in the solid-state. J. Pharm. Sci. 100, 1607–1617. https://doi.org/10.1002/jps.22405.

Sun, D.D., Wen, H., Taylor, L.S., 2016. Non-sink dissolution conditions for predicting product quality and in vivo performance of supersaturating drug delivery systems. J. Pharm. Sci. 105, 2477–2488. https://doi.org/10.1016/j.xphs.2016.03.024.

Tachibana, T., Nakamura, A., 1965. A methode for preparing an aqueous colloidal dispersion of organic materials by using water-soluble polymers: dispersion of b-carotene by polyvinylpyrrolidone. Kolloid-Zeitschrift und Zeitschrift für Polymere 203, 130–133. https://doi.org/10.1007/BF01507758.

Tambe, S., Jain, D., Meruva, S.K., Rongala, G., Juluri, A., Nihalani, G., Mamidi, H.K., Nukala, P.K., Bolla, P.K., 2022. Recent advances in amorphous solid dispersions: preformulation, formulation strategies, technological advancements and characterization. Pharmaceutics 14, 2203. https://doi.org/10.3390/pharmaceutics14102203.

Thakral, N.K., Behme, R.J., Aburub, A., Peterson, J.A., Woods, T.A., Diseroad, B.A., Suryanarayanan, R., Stephenson, G.A., 2016. Salt disproportionation in the solid state: role of solubility and counterion volatility. Mol. Pharmaceutics 13, 4141–4151. https://doi.org/10.1021/acs.molpharmaceut.6b00745.

Wang, C., Rosbottom, I., Turner, T.D., Laing, S., Maloney, A.G., Sheikh, A.Y., Docherty, R., Yin, Q., Roberts, K.J., 2021. Molecular, solid-state and surface structures of the conformational polymorphic forms of ritonavir in relation to their physicochemical properties. Pharm. Res. 38, 971–990. https://doi.org/10.1007/s11095-021-03048-2.

Wong, J.J.L., Yu, H., Lim, L.M., Hadinoto, K., 2018. A trade-off between solubility enhancement and physical stability upon simultaneous amorphization and nanonization of curcumin in comparison to amorphization alone. Eur. J. Pharm. Sci. 114, 356–363. https://doi.org/10.1016/j.ejps.2018.01.010.

Xu, H., Vela, S., Shi, Y., Marroum, P., Gao, P., 2017. In vitro characterization of ritonavir drug products and correlation to human in vivo performance. Mol. Pharmaceutics 14, 3801–3814. https://doi.org/10.1021/acs.molpharmaceut.7b00552.

Xu, H., Krakow, S., Shi, Y., Rosenberg, J., Gao, P., 2018. In vitro characterization of ritonavir formulations and correlation to in vivo performance in dogs. Eur. J. Pharm. Sci. 115, 286–295. https://doi.org/10.1016/j.ejps.2018.01.026.

Yao, X., Henry, R.F., Zhang, G.G., 2022. Ritonavir form III: a new polymorph after 24 years. J. Pharm. Sci. 112, 237–242. https://doi.org/10.1016/j.xphs.2022.09.026.

Yu, J., Yu, D., Lane, S., McConnachie, L., Ho, R.J., 2020. Controlled solvent removal from antiviral drugs and excipients in solution enables the formation of novel combination multi-drug-motifs in pharmaceutical powders composed of lopinavir, ritonavir and tenofovir. J. Pharm. Sci. 109, 3480–3489. https://doi.org/10.1016/j.xphs.2020.08.003.

Zannou, E.A., Ji, Q., Joshi, Y.M., Serajuddin, A.T., 2007. Stabilization of the maleate salt of a basic drug by adjustment of microenvironmental pH in solid dosage form. Int. J. Pharm. 337, 210–218. https://doi.org/10.1016/j.ijpharm.2007.01.005.

Zhang, Z., Dong, L., Guo, J., Li, L., Tian, B., Zhao, Q., Yang, J., 2021. Prediction of the physical stability of amorphous solid dispersions: relationship of aging and phase separation with the thermodynamic and kinetic models along with characterization techniques. Expert Opin. Drug Deliv. 18, 249–264. https://doi.org/10.1080/17425247.2021.1844181.